Structural Transformations in Oxide Ceramic Coatings Formed on Aluminum Alloys in Silicate Electrolyte

Volodymyr Posuvailo, Ihor Koval'chuck, Iryna Ivasenko, Yurii Kanyuk, and Roman Iurkevych

Abstract X-ray phase analysis of oxide ceramic coatings formed on the alloys D16T and AK9M2 in the process of plasma electrolyte oxidation in the electrolyte (KOH (3 g/l), Na_2SiO_3 (2 g/l) is fulfilled. It is established that at the beginning of the coating synthesis (after 5 min) there is a transformation of the crystal lattice of aluminum with the formation of the compound $Al_{3.21}Si_{0.47}$ in the surface layers of both alloys. After 1 h of synthesis, the corresponding oxide ceramic coatings on alloys D16T and AK9M2 contain the following phases: α-Al_2O_3 (corundum), γ-Al_2O_3, and $Al_2O_3 \cdot SiO_2$ (sillimanite). When increasing the synthesis time to 2 h there is a partial conversion of sillimanite ($Al_2O_3 \cdot SiO_2$) to mullite ($3Al_2O_3 \cdot 2SiO_2$) in the coatings on the alloy AK9M2. The study of the surface microstructure showed a uniform growth of oxide ceramic coatings and an increase of Si areas due to the formation of SiO_2 and the formation of a low-temperature substitution compound $Al_{3.21}Si_{0.47}$. The image segmentation method was used to analyze the pore sizes and the distribution and size of bit channels. It is established that the minimum pore size is approximately 0.9 μm.

V. Posuvailo (✉) · I. Koval'chuck · I. Ivasenko · Y. Kanyuk
Karpenko Physico-Mechanical Institute of the NASU, Lviv, Ukraine
e-mail: vposuvailo@gmail.com

I. Koval'chuck
e-mail: ihor-kovalchuk@i.ua

I. Ivasenko
Lviv Polytechnic National University, Lviv, Ukraine

R. Iurkevych
Hetman Petro Sahaidachnyi National Army Academy, Lviv, Ukraine

O. Fesenko and L. Yatsenko (eds.), *Nanostructured Surfaces, Nanocomposites and Nanomaterials, and Their Applications*, Springer Proceedings in Physics 296,
https://doi.org/10.1007/978-3-031-42704-6_3

1 Introduction

An urgent task of modern science and technology is the development of new technologies for the formation of highly effective, reliable coatings for the protection and strengthening of metal products. There are many ways of increasing the wear and corrosion resistance of light alloys [1–10]: anodizing, chromium plating, phosphating, oxidation, nitriding, etc. One of these methods is plasma electrolyte oxidation. Therefore, a new type of surface treatment and strengthening of metal materials, which is a variant of traditional anodizing pro-plasma electrolytic oxidation (PEO), is actively developing. It makes it possible to obtain multifunctional oxide ceramic coatings with a unique set of properties on valve metals (Al, Mg, Ti, Zr, Ta) [11–13]. However, in addition to high corrosion resistance, oxide ceramic coatings should also have good wear resistance. There are four main stages of the formation of oxide ceramic coatings [14] on valve metals: the formation of the primary oxide film at the pre-spark stage by an electrochemical mechanism; breakdown of the primary oxide film and the appearance of a plasma clot in the discharge channel; plasma chemical reactions of formation of intermediate and final products; and condensation and polymorphic transformations of oxide phases [14]. In recent years, this method has been actively used to form wear- and corrosion-resistant coatings on silumins, which are widely used in industry and contain 4…0.22 mass % of silicon [15–17]. Silumins have a low cost, and they are widely used in various industries, namely: in mechanical engineering (pistons, body parts, engine cylinders), aircraft construction (cylinder blocks, pistons for cooling, aviation assemblies), aerospace engineering (parts with a low temperature coefficient of linear expansion and a high level of mechanical properties), during the manufacture of gas turbine equipment (generators, heat exchangers), etc. Their corrosion resistance is higher than that of deformable aluminum alloys, but at the same time their wear resistance is not high. In the last decade, methods of applying PEO coatings on deformable aluminum alloys and silumins have been actively developed.

The purpose of this work was to establish the mechanism of interaction of plasma discharge channels with aluminum and silicon and the effect of silicon on the phase composition, crystal structure, and porosity of oxide ceramic coatings synthesized on aluminum alloys of the Al–Si and Al–Cu systems.

2 Methods and Materials

Oxide ceramic coatings were synthesized on aluminum alloys AK9M2 and (Al—87.6–93.6%, Si—6–8%, Cu—1.5%, Mg—0.2–0.5%, Mn—0.2–0.5%) and D16 (94.7% Al; 3.8…4.9 Cu; 1.2…1.8 Mg; 0.3…0.9% Mn). The size of the samples is 20 * 15 * 3 mm. Before synthesis, the samples were polished and washed in distilled water and ethyl alcohol. The coating was formed by alternately applying anodic and cathodic pulses to the sample. The coatings were synthesized at cathodic to anodic

current densities ratio $j_c/j_a = 15/15$ A/dm^2 for time 5 min and 2 h. An aqueous solution of KOH (3 g/l), Na_2SiO_3 (2 g/l) served as the electrolyte. A DRON-3.0 diffractometer with CuK_α radiation was used for X-ray phase analysis of coatings. The content of each of the phases was determined by diffractograms using the FullProf program package, using the multi-disciplinary method of Rietveld [18]. Porosity was investigated by analyzing microphotographs of PEO coatings obtained on a Zeiss EVO-40XVP scanning electron microscope with a magnification of ×500 times according to the method [19].

3 Results and Discussions

X-ray structural analysis was used to determine the silicon content in the original AK9M2 alloy, as well as the composition of the corresponding oxide ceramic coatings after 5 min and 2 h of PEO treatment. The corresponding X-ray diffractograms of the original AK9M2 alloy and the oxide ceramic coating on it after 5 min of processing are shown in Fig. 1.

According to X-ray images, it was established that the intensity of Al, Si reflexes decreases after PEO treatment of the AK9M2 alloy. In addition, traces of impurity phases such as SiO_2 and $Al_{2.67}O_4$ were found in the coatings. It was established for the first time that already at the beginning of the synthesis of the oxide ceramic coating, aluminum and silicon form $Al_{4-x}Si_x$ substitution compounds. In particular, the substitution compound $Al_{3.21}Si_{0.47}$ has space group $Fm3m$ and lattice parameters $a = 0.5641$ nm [20]. Its presence is confirmed by the decrease in intensity of Al and Si reflexes and their increase for $Al_{4-x}Si_x$.

Figure 2 shows X-ray diffraction patterns of alloy D16 after 5 min of PEO treatment.

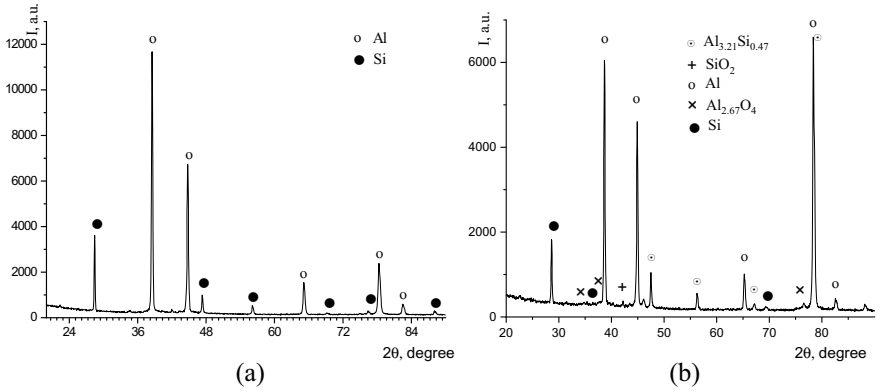

Fig. 1 X-ray diffraction of initial alloy AK9M2 (**a**) and oxide ceramic coatings after 5 min synthesis on AK9M2 (**b**)

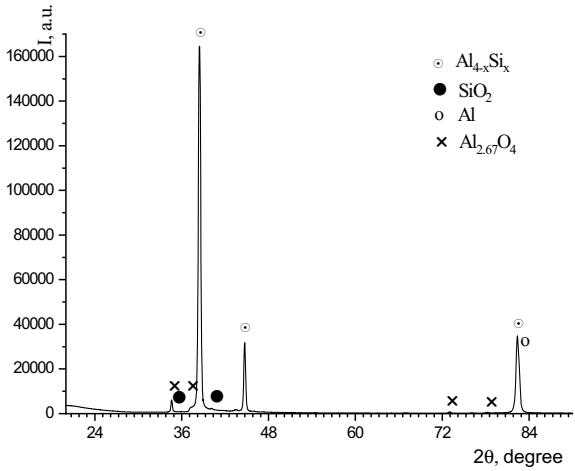

Fig. 2 X-ray diffraction of oxide ceramic coatings on D16 alloy after 5 min synthesis

On the surface of D16 alloy after 5 min of PEO treatment, in addition to Al, substitution compounds $Al_{4-x}Si_x$ as well as traces of impurity phases $Al_{2.67}O_4$ and SiO_2 were detected.

This indicates that silicon is reduced from the electrolyte (Na_2SiO_3) with subsequent synthesis of the $Al_{4-x}Si_x$ compound in the plasma discharge channels on the surface of the alloy.

The works [14, 21, 22] showed the growth mechanisms of the oxide ceramic coating on aluminum alloys in the process of plasma electrolytic oxidation. As you know, valve metals (Al, Ti, Mg, Zr, Ta) are usually covered with a thin passive oxide film. Due to the application of high voltage, this film breaks down and discharge plasma channels appear. Atomization and ionization of the electrolyte and base metal from which the oxide ceramic coating grows take place in them.

Previously, an analysis of the distribution of silicon in oxide ceramic coatings was carried out [23]. In particular, it was established that the transition layer between the aluminum base and oxide ceramics contains up to 0.5 at. % silicon and is partially amorphized. Al_2SiO_5 and $Al_6Si_2O_{13}$ phases are formed in the near-electrolyte region.

The main phases of oxide ceramic coatings are γ-Al_2O_3 (*Fm*3*m*) and α-Al_2O_3 (*R*-3*C*). The formation of α-Al_2O_3 (corundum) occurs when the temperature in the vicinity of the discharge channel rises above 1000 K to the temperature of the phase transition of γ-Al_2O_3 to α-Al_2O_3. The increase in corundum content in oxide ceramic coatings grows with increasing thickness and decreasing thermal conductivity of the coatings [24].

In works [25, 26] the growth mechanisms of oxide ceramic coatings on alloys of the Al–Si system were given. In particular, it was established that the coating begins to form at the boundary of the Al and Si phase distribution from the passivation of aluminum and silicon, the oxide film on aluminum breaks down, and the oxide ceramic coating begins to grow when the dielectric properties of aluminum oxide and silicon oxide are equalized. Corresponding oxide ceramic coatings consist of

γ-Al_2O_3 and α -Al_2O_3 and a small amount of SiO_2 and Al_2SiO_5. It should be noted that these coatings are synthesized at a much lower current density (4–6 A/dm^2) and in the presence of a phosphate electrolyte. Therefore, the increase in current density up to 15 A/dm^2 can also affect the coating formation mechanism. In Fig. 3 the following photographs of the AK9M2 alloy surface after 5 min of synthesis of the oxide ceramic coating were obtained using optical (a) and electron microscopes (b).

The alloy AK9M2 contains silicon in the form of lamellar inclusions. In Fig. 3a a photomicrograph of the AK9M2 surface is shown, where the inclusions have a characteristic dendritic structure. Based on the X-ray phase analysis of the oxide ceramic coating (Fig. 1b), this can be explained by the formation of SiO_2 oxide on silicon. In Fig. 3b the given micrograph of the same surface was made with the help of an electron microscope at a magnification of $\times$500. It has elongated (elongated) pores (black areas) of large size, which were formed at the Al–Si interface.

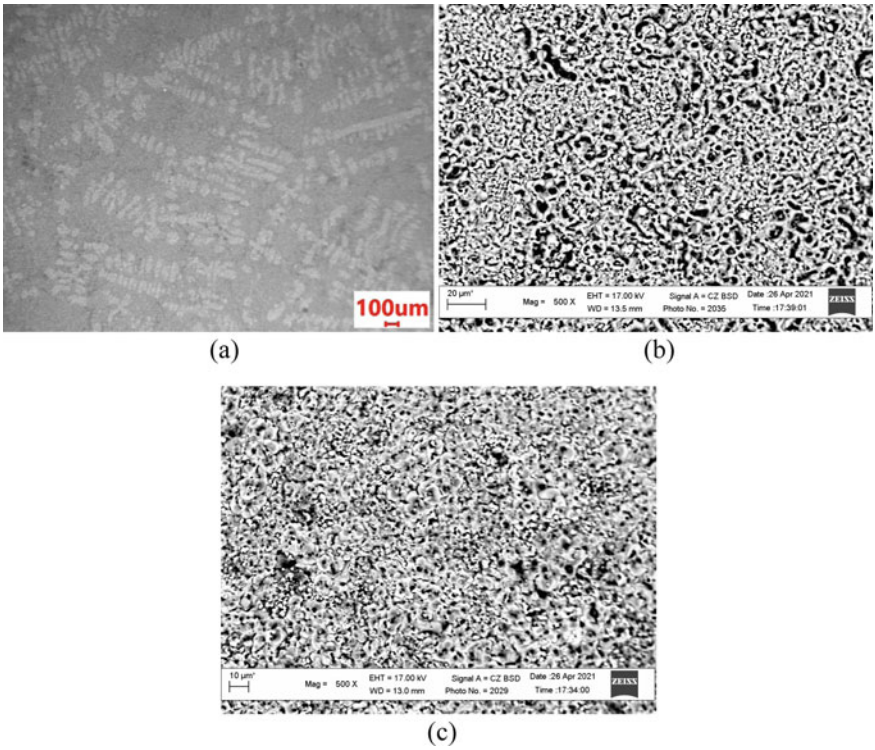

Fig. 3 Surfaces of oxide ceramic coatings on AK9M2 (**a**, **b**) and D16T (**c**) alloy after 5 min PEO synthesis

Table 1 Segmentation results of surface defects

	D16 X500_BSD	AK9M2 X500_BSD
N	9881	13,062
S_{def}, m^2	1.98×10^{-8}	3.10×10^{-8}
N/S_{surf}, 1/m^2	4.72×10^{10}	6.24×10^{10}
S_{def}/S_{surf}	0.095	0.15
S_{min}, m^2	5.16×10^{-14}	2.07×10^{-13}
S_{max}, m^2	4.14×10^{-11}	9.16×10^{-11}
S_{av}, m^2	2.01×10^{-12}	2.27×10^{-12}

The surface of the D16 alloy (Fig. 3c) under the same conditions of synthesis of the oxide ceramic coating has a significantly different structure. Larger pores, which are formed within the first 5 min of synthesis, are caused by the presence of $CuMgAl_2$ and $CuAl_2$ intermetallics in the D16 alloy. They are significantly smaller in size and round in shape, unlike the lamellar silicon inclusions in the AK9M2.

Image segmentation was performed by thresholding of image intensity function. The operation of thresholding consists in comparing the value of the image intensity function of each pixel of the image with a given threshold value. The selection of the appropriate value makes it possible to select areas of a certain type on the image. In the binarization process, the initial grayscale image, which has 256 Gy levels, is transformed into black and white, where the background pixels have a value of 1, and the pore pixels have a value of 0 (see Fig. 3). In the case of a noisy background, a filtering procedure can be applied before segmentation [27–29].

The defect parameters were determined by the segmentation procedure, where the total number of defects is N; defect area S_{def}; the ratio of the number of defects to the total area N/S_{pov}; the ratio of the area of defects to the total area S_{def}/S_{pov}; minimum defect size S_{min}; maximum defect size S_{max}; and average defect size S_{avg}. Square of surface is $S_{pov} = 2.09 \times 10^{-7}$ m^2. Defect parameters are given in Table 1.

Oxide ceramic coatings on the AK9M2 alloy have a significantly larger number of pores and more than twice their maximum size compared to the corresponding coatings on the D16 alloy. The obtained results correlate with [26], where the pore sizes in the oxide ceramic coating on Z10L9 silumin are 3.61 ± 1.31 μm and are much larger than on aluminum (1.06 ± 0.47 μm).

The analysis of the emission spectra of the electrolytic plasma at the initial time of synthesis indicates the presence in them of the emission lines of Cu on the D16 alloy and Si on the silumins. This can be explained by the occurrence of spark discharge channels in the areas with the lowest dielectric properties and the defective structure that occurs in the places where the inclusions come to the surface.

Figure 4 shows the diffractograms of oxide ceramic coatings on AK9M2 and D16 alloys after 2 h of coating synthesis. The quantitative content of phases calculated by the complete profile method of Rietveld using the FullProf program is given in Table 2.

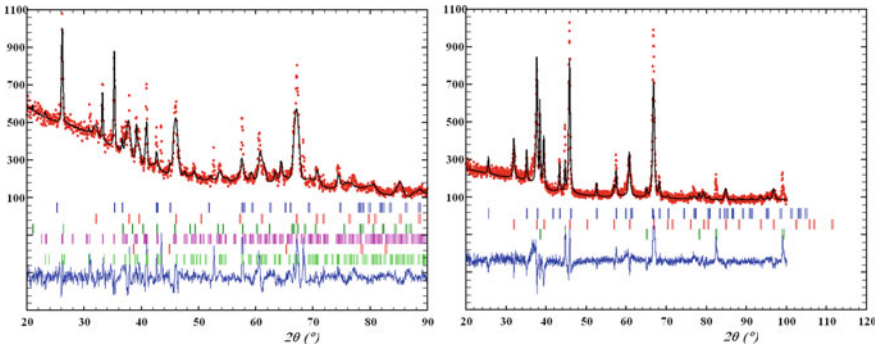

Fig. 4 X-ray diffraction patterns of ceramic oxide coatings obtained on AK9M2 and D16 alloys after 2 h

Table 2 Phase composition of oxide ceramic coatings obtained on AK9M2 and D16 alloys

AK9M2		D16
Phase	Content, mass%	Content, mass%
α-Al_2O_3	11.28	17.48
γ-Al_2O_3	44.45	73.29
SiO_2	3.08	–
$Al_2O_3 \cdot SiO_2$	40.12	–
Al	1.07	9.23

The main phases in coatings on AK9M2 alloy are γ-Al_2O_3 and sillimanite—$Al_2O_3 \cdot SiO_2$, and on D16 alloy γ-Al_2O_3 and α-Al_2O_3. It should be noted that the content of corundum and sillimanite in oxide ceramic coatings increases with increasing time of coating synthesis.

Based on the phase analysis of oxide ceramic coatings and their surface, the effect of silicon on structural transformations in aluminum alloys of the Al–Si and Al–Cu systems was established. In particular, in both cases, at the beginning of the synthesis of the oxide ceramic coating, a transition compound $Al_{4-x}Si_x$ and SiO_2 is formed, which contributes to the formation of a uniform coating and the reduction of the breakdown voltage.

The content of these phases is significantly higher in the alloy with a high silicon content than on the alloy of the Al–Cu system. As the synthesis time increases, its influence changes significantly. In silumins, silicon is included in the composition of sillimanite and silicon oxide, and in alloys of the Al–Cu system of silicon, only traces of silicon are observed in the near-electrolyte region of the coating.

4 Conclusions

X-ray structural analysis revealed that during plasma electrolytic oxidation of alloys of the Al–Si and Al–Cu systems in an alkaline silicate electrolyte, a number of structural transformations occur in the oxide ceramic layers. In particular, it is shown that $Al_{4-x}Si_x$ compounds form already within 5 min of synthesis on both aluminum and silicon alloys. The segmentation method was used to analyze oxide ceramic coatings on two doping systems. After 5 min of synthesis of the oxide ceramic coating on the AK9M2 alloy, a larger size of pores in the coating was recorded, and its maximum porosity was 14.8%. Most likely, they are formed at the aluminum–silicon interface and have a characteristic oblong shape. In the coating on the D16 alloy under the same synthesis conditions, the porosity is 9.5%. During 2 h of synthesis, the influence of silicon on alloys increases significantly. Only traces of silicon are observed in the oxide ceramic coating on the D16 alloy, while $Al_2O_3 \cdot SiO_2$ (sillimanite) and $3Al_2O_3 \cdot 2SiO_2$ (mullite) are formed on AK9M2. Therefore, in the plasma discharge channels on the surface of both alloys, silicon is reduced from the electrolyte (Na_2SiO_3) with subsequent synthesis of $Al_{4-x}Si_x$ compounds.

References

1. M.M. Student et al., Influence of the composition of electrolyte for hard anodizing of aluminium on the characteristics of oxide layer. Mater. Sci. **57**, 240–247 (2021)
2. V.I. Pokhmurskii, I.M. Zin, V.A. Vynar, L.M. Bilyy, Contradictory effect of chromate inhibitor on corrosive wear of aluminium alloy. Corros. Sci. **53**, 904–908 (2011)
3. V.I. Pokhmurskii, I.M. Zin, V.A. Vynar, O.P. Khlopyk, L.M. Bilyy, Corrosive wear of aluminium alloy in presence of phosphate. Corros. Eng. Sci. Technol. **47**, 182–187 (2012)
4. V. Hutsaylyuk, M. Student, K. Zadorozhna, P. Maruschak, H. Pokhmurska, Improvement of wear resistance of aluminum alloy by HVOF method. J. Market. Res. **9**, 16367–16377 (2020)
5. V. Kyryliv, B. Chaikovs'kyi, O. Maksymiv, B. Mykytchak, Fatigue and corrosion fatigue of roll steels with surface nanostructure. J. Nano Res. **51**, 92–97 (2018)
6. I.M. Zin, O.P. Khlopyk, M.Ya. Holovchuk, Protective action of inorganic inhibitors on mechanically activated aluminum surfaces. Mater. Sci. **49**, 298–303 (2013)
7. I. Pohrelyuk, O. Yaskiv, O. Tkachuk, D.B. Lee, Formation of oxynitride layers on titanium alloys by gas diffusion treatment. Met. Mater. Int. **15**, 949–953 (2009)
8. K. Szymkiewiccz et al., Effect of nitriding conditions of Ti6Al7Nb on microstructure of TiN surface layer. J. Alloy. Compd. **845**, 156320 (2020)
9. I.M. Pohrelyuk, O.V. Tkachuck, R.V. Proskurnyak, Corrosion resistance of the Ti–6Al–4V titanium alloy with nitride coatings in 0.9% NaCl. JOM **63**, 35–40 (2011)
10. I. Pohrelyuk, J. Morgel, O. Tkachuk, K. Szymkiewiccz, Effect of temperature on gas oxynitiding of Ti–6Al–4V alloys. Surf. Coat. Technol. **360**, 103–109 (2019)
11. Y.G. Gutsalenko, E.K. Sevidova, I.I. Stepanova, Evaluation of technological capability to form dielectric coatings on AK6 alloy, using method of microarc oxidation. Surf. Eng. Appl. Electrochem. **55**, 602–606 (2019)
12. M.M. Student, V.M. Posuvailo, H.H. Veselivs'ka, Y.Y. Sirak, R.A. Yatsyuk, Corrosion resistance of plasma-electrolytic layers on alloys coatings of Al–Cu–Mg system for various modes of heat treatment. Mater. Sci. **53**, 789–795 (2018)

13. H.M. Nykyforchyn, V.S. Agarwala, M.D. Klapkiv, V.M. Posuvailo, Simultaneous reduction of wear and corrosion of titanium, magnesium and zirconium alloys by surface plasma electrolytic oxidation treatment. Adv. Mater. Res. **38**, 27–35 (2008)
14. M.D. Klapkiv, Simulation of synthesis of oxide-ceramic coatings in discharge channels of a metal-electrolyte system. Mater. Sci. **35**, 279–283 (1999)
15. H.V. Karakurkchi, M.D. Sakhnenko, M.V. Ved, S.I. Zyubanova, I.I. Stepanova, Corrosion and physicomechanical properties of the coatings on Ak12m2mgn alloy formed by plasma-electrolytic oxidation. Mater. Sci. **55**, 693–702 (2020)
16. G. Li, F. Ma, Z. Li, Y. Xu, F. Gao, L. Guo, J. Zhu, G. Li, Y. Xia, Influence of applied frequency on thermal physical properties of coatings prepared on Al and AlSi alloys by plasma electrolytic oxidation. Coatings **11**, 1439 (2021)
17. A.V. Polunin, P.V. Ivashin, I.A. Rastegaev, E.D. Borgardt, M.M. Krishtal, Wear resistance of the oxide layers formed on AK9pch silumin by microarc oxidation in an electrolyte modified by silicon dioxide nanoparticles, in *Russian Metallurgy (Metally)* (2016), pp. 385–388
18. J. Rodríguez-Carvajal, *Program FullProf.2k. Version 2.20* (Laboratoire Léon Brillouin (CEA–CNRS), France, 2002).
19. I. Ivasenko, V. Posuvailo, M. Klapkiv, V. Vynar, S. Ostap'yuk, Express method for determining the presence of defects of the surface of oxide-ceramic coatings. Mater. Sci. **45**, 460–464 (2009)
20. M. Senoo, H. Mii, I. Fujishiro, T. Fujikawa, Precise measurements of lattice compression of Al, Si and Al-Si alloys by high pressure X-ray diffractometry. Jpn. J. Appl. Phys. **15**, 871–880 (1976)
21. R.O. Hussein, X. Nie, D.O. Northwood, An investigation of ceramic coating growth mechanisms in plasma electrolytic oxidation (PEO) processing. Electrochim. Acta **112**, 111–119 (2013)
22. T.W. Clyne, S.C. Troughton, A review of recent work on discharge characteristics during plasma electrolytic oxidation of various metals. Int. Mater. Rev. **64**, 127–162 (2018)
23. F. Monfort et al., Development of anodic coatings on aluminium under sparking conditions in silicate electrolyte. Corros. Sci. **49**, 672–693 (2007)
24. P. Leone, A. Nominé, D. Veys-Renaux, G. Henrion, T. Belmonte, J. Martin, Influence of electrolyte ageing on the plasma electrolytic oxidation of aluminium. Surf. Coat. Technol. **269**, 36–46 (2015)
25. L. Wang, X. Nie, Silicon effects on formation of EPO oxide coatings on aluminum alloys. Thin Solid Films **494**, 211–218 (2006)
26. H. Yu, Q. Dong, Y. Chen, C. Chen, Influence of silicon on growth mechanism of micro-arc oxidation coating on cast Al–Si alloy. R. Soc. Open Sci. **5**, 172428 (2018)
27. R.M. Palenichka, P. Zinterhof, I.B. Ivasenko, Adaptive image filtering and segmentation using robust estimation of intensity, in *Lecture Notes in Computer Science*, vol. 1876 (2000)
28. R.M. Palenichka, P. Zinterhof, Y.B. Rytsar, I.B. Ivasenko, Structure-adaptive image filtering using order statistics. J. Electron. Imaging **7**, 339–349 (1998)
29. R. Vorobel, I. Ivasenko, O. Berehulyak, Automatized computer system for evaluation of rust using modified single-scale retinex, in *Proceedings of 1st Ukraine Conference on Electrical and Computer Engineering*, UKRCON 2017, Kyiv, Ukraine (2017), pp. 1002–1006